IEEE Access
Multidisciplinary ⋮ Rapid Review ⋮ Open Access Journal

Received February 3, 2020, accepted February 15, 2020, date of publication March 26, 2020, date of current version April 27, 2020.

Digital Object Identifier 10.1109/ACCESS.2020.2983541

Influence of Extension Length of Rotor End Windings on the Three-Dimensional Electromagnetic Field and Temperature Rise in the Large Turbine Generator End Zone With Magnetic Screen

HAN JICHAO[1], WANG CHAO[1], WANG YANG[1], SUN YUTIAN[2], AND ZHENG PING[3]

[1]School of Electrical and Electronic Engineering, Harbin University of Science and Technology, Harbin 150080, China
[2]Harbin Institute of Large Electrical Machinery, Harbin 150040, China
[3]Harbin Institute of Technology, Harbin 150001, China

Corresponding author: Han Jichao (hanjichao163@163.com)

This work was supported in part by the National Natural Science Foundation of China under Grant 51807043, in part by the Postdoctoral Foundation of Heilongjiang Province of China under Grant LBH-TZ1005, in part by the Fundamental Research Foundation for Universities of Heilongjiang Province under Grant 2019-KYYWF-0209, in part by the China Postdoctoral Science Foundation under Grant 2018T110269, in part by the China Postdoctoral Science Foundation under Grant 2018M630336, in part by the Fundamental Research Foundation for Universities of Heilongjiang Province under Grant LGYC2018JC024, in part by the University Nursing Program for Young Scholars with Creative Talents in Heilongjiang Province under Grant UNPYSCT-2017080, in part by the Postdoctoral Foundation of Heilongjiang Province of China under Grant LBH-Z17040, and in part by the Heilongjiang Science and Technology Achievement Conversion and Cultivation Project under Grant TSTAU-R2018004.

ABSTRACT Leakage magnetic field from the rotor end windings affects obviously the electromagnetic losses and temperature of end components in the turbine generator end zone with magnetic screen. As the capacity of turbine generator increases, this effect of rotor end windings has become more prominent. To investigate influence of the extension length of rotor end windings on the electromagnetic and thermal fields in the turbine generator end zone with magnetic screen, three-dimensional transient electromagnetic field model of 1250 MW turbine generator end zone is given. Leakage magnetic field and losses of end components are compared and studied in the end zone under the different extension lengths of rotor end windings. Based on the calculation results of electromagnetic losses (heat sources) and flow network (boundary conditions), three-dimensional fluid-thermal coupling field is calculated in the turbine generator end zone with magnetic screen. Distribution of complex fluid velocity in the end zone is obtained. Influence of the different extension lengths of rotor end windings on the stator-end copper coil, screen plate, finger plate, press plate, magnetic screen, and stator end core is researched in the turbine generator end zone. The accuracy of calculation results is validated by experimental values.

INDEX TERMS Turbine generator end zone, magnetic screen, rotor end windings, extension length, transient electromagnetic field, thermal field.

I. INTRODUCTION

Size of the end windings has a great effect on the electromagnetic losses and temperature rise of end components in the turbine generator end zone with magnetic screen. The current in the stator and rotor end windings of large turbine generator is large, which leads to a high leakage magnetic field and losses of the end components in the turbine generator end zone with magnetic screen. If the structure design of the turbine generator end zone with magnetic screen is inappropriate, the leakage magnetic field, losses, and temperature of the end components become higher. It will affect seriously the safety and stability of turbine generator. Accurate calculation of the leakage magnetic field, losses, and temperature of the end components in the large turbine generator end zone with magnetic screen has an important engineering significance.

The total leakage flux in the end zone of the turbine generator is formed by the interaction of the leakage flux

The associate editor coordinating the review of this manuscript and approving it for publication was Yi Ren.

from the stator end windings and the leakage flux from the rotor end windings. The extension length of rotor end windings affects the distribution and strength of the total leakage flux in the turbine generator end zone with magnetic screen. Furthermore, the losses and temperature distribution of the end components are changed with the extension length of rotor end windings. Reasonable design of the extension length of rotor end windings could reduce effectively the losses and temperatures of the end metal components, which improves obviously the heat resistance of the large turbine generator. Therefore, it is of great importance for large turbine generator to study influence of the different extension lengths of rotor end windings on the electromagnetic field, losses, and temperature distribution of the end components in the complex turbine generator end zone with magnetic screen.

The analysis of the electromagnetic field, fluid flow, and temperature distribution is necessary to the design of the turbine generator. Extensive studies are performed on the multi-physics field in the turbine generator. Albanese *et al.* focused on the coupled numerical calculations of the forces and stresses on the end winding of turbine generator [1]. Fujita *et al.* performed the eddy current analysis in the stator end structures of large capacity turbine generators [2]. Xu *et al.* studied the influence of rotor damping structure on speed fluctuation and asynchronous operating ability of the turbine generators with loss of excitation [3]. Fratila *et al.* performed the iron loss calculation in a turbine generator using finite element method [4]. Šašić *et al.* focused on the finite element analysis of turbine generator rotor winding shorted turns [5]. Sufei *et al.* studied the implementation of surface impedance boundary conditions, impact of press plate structure on the flux and loss distributions, efficient calculation of the strand eddy current loss distributions, parametric study for the design, and fast calculation of the magnetic field and loss distributions in the end region of large synchronous generators [6]–[10]. Some other experts also studied the multi-physics field of turbine generator [11]–[14], but very few focused on the influence of the extension length of rotor end windings on the electromagnetic losses, fluid flow, and thermal field in the large turbine generator end zone with magnetic screen.

In this paper, three-dimensional transient electromagnetic field model of 1250 MW turbine generator end zone with magnetic screen is established. The electromagnetic field and losses of end components are obtained in the turbine generator end zone under the different extension lengths of rotor end windings. Three-dimensional fluid-thermal coupling model of the large turbine generator end zone with magnetic screen is given. Loss values of the end components from three-dimensional transient electromagnetic field are applied to end zone as heat source under the different extension lengths of rotor end windings. Fan outlet pressure and inlet velocity from flow network are applied to end zone as boundary conditions. The fluid field and thermal field in the turbine generator end zone with magnetic screen are calculated by the finite volume method. The distribution of

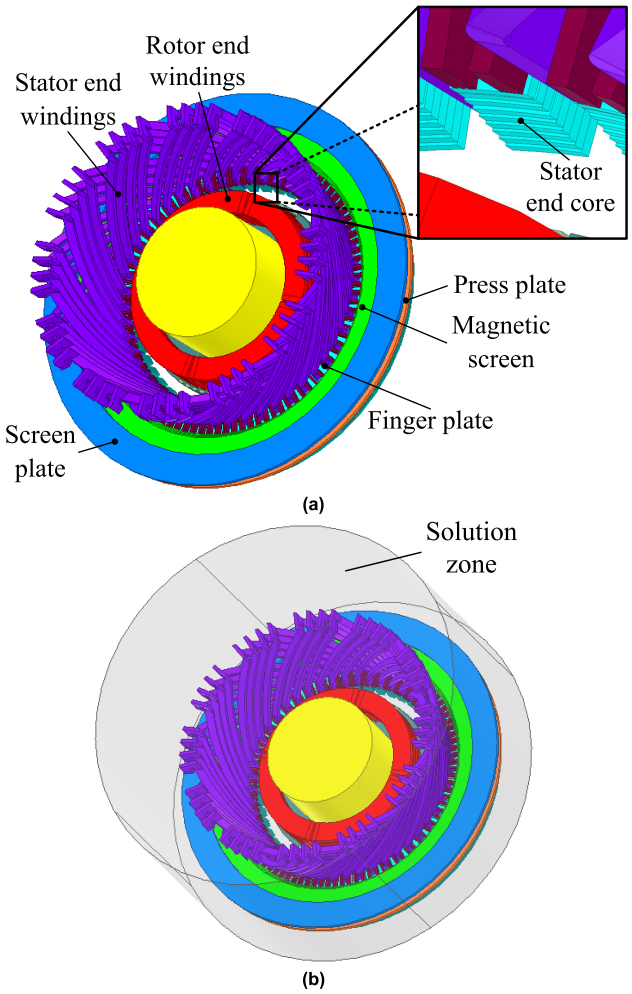

FIGURE 1. Solving model of the three-dimensional transient electromagnetic field in the turbine generator end zone with magnetic screen. (a) End components. (b) Electromagnetic solution zone.

fluid velocity around the finger plate is determined. Influence of the different extension lengths of rotor end windings on the electromagnetic losses and temperature distribution of the end components is studied in the large turbine generator end zone with magnetic screen, which could provide the important reference for the optimization design of the turbine generator end zone.

II. ANALYSIS OF ELECTROMAGNETIC FIELD IN THE END ZONE OF TURBINE GENERATOR

In this paper, the mathematical model of three-dimensional transient electromagnetic field of 1250 MW turbine generator end zone with magnetic screen are established [15], [16]. Fig. 1 shows the solving model of the three-dimensional transient electromagnetic field in the turbine generator end zone with magnetic screen. Fig. 1(a) gives the end components of the turbine generator. Fig. 1(b) gives the electromagnetic solution zone. The electromagnetic solution zone is divided into the eddy current zone and the non eddy current zone.

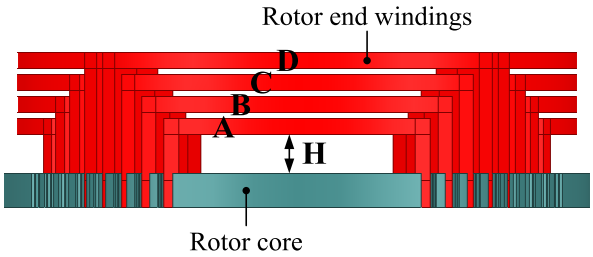

FIGURE 2. Location of rotor core and rotor end windings.

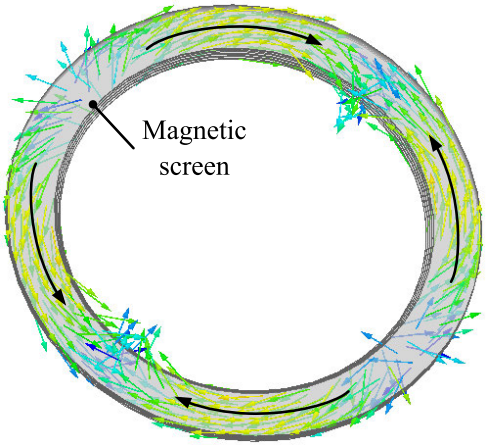

FIGURE 3. Magnetic flux vector within the magnetic screen when the extension length of rotor end windings is H=205 mm.

Eddy current zone:

$$\begin{cases} \nabla \cdot \mu \left(\boldsymbol{T} - \nabla \psi \right) = -\nabla \cdot \mu \boldsymbol{H}_s \\ \nabla \times \rho \, \nabla \times \boldsymbol{T} - \nabla \rho \, \nabla \cdot \boldsymbol{T} + \dfrac{\partial \mu (\boldsymbol{T} - \nabla \psi)}{\partial t} + \dfrac{\partial \mu \boldsymbol{H}_s}{\partial t} = 0 \end{cases} \tag{1}$$

Non eddy current zone:

$$\boldsymbol{H}_s = \frac{1}{4\pi} \int_{\Omega_s} \frac{\boldsymbol{J}_s \times \boldsymbol{r}}{r^3} d\Omega \tag{2}$$

$$\nabla \cdot \mu \nabla \psi = \nabla \cdot \mu \boldsymbol{H}_s \tag{3}$$

where μ is the permeability (in H/m), $\boldsymbol{T}$ the electric vector potential, $\boldsymbol{J}_s$ is the source current density in the winding (in A/m^2), ρ is the resistivity (in $\Omega \cdot$ m), t is the time (in s), and ψ is the scalar magnetic potential.

For the convenience of study, the rotor end windings are marked as A, B, C and D along the axial direction. The distance between the rotor end windings keeps constant. The distance between the rotor end winding (A) and the rotor core is denoted as H. The distance between the rotor end winding (A) and the rotor core means the extension length of rotor end windings in this paper. Fig. 2 shows the location of rotor core and rotor end windings. The complex three-dimensional electromagnetic field, fluid field, and temperature field in the end zone of turbine generator are studied in detail when the extension length of rotor end windings is adjusted to H=45 mm, H=85 mm, H=125 mm, H=165 mm, and H=205 mm, respectively. Fig. 3 gives the distribution

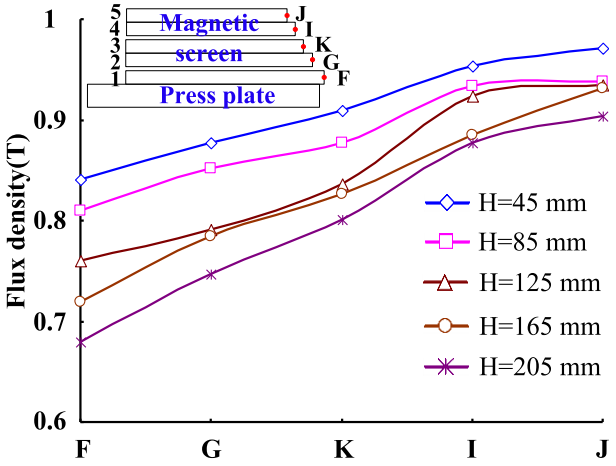

FIGURE 4. Flux density on the inner surface of the magnetic screen at position F, position G, position K, position I, and position J under the different extension lengths of rotor end windings.

of the leakage magnetic field in the end zone of the turbine generator when the extension length of rotor end windings is H=205 mm.

The simulation time of the 3-D transient electromagnetic field model is about 31 hours. Fig. 3 gives the magnetic flux vector within the magnetic screen when the extension length of rotor end windings is H=205 mm. The magnetic flux vector within magnetic screen presents a trend of two-in and two-out. The reason for this is that the pole number of this turbine generator is four.

The eddy current losses of end components can be determined as follows:

$$P_e = \frac{1}{T_t} \int \sum_{e=1}^{k} J_e^2 \Delta_e \sigma_r^{-1} dt \tag{4}$$

where T_t is the period of time (in s), σ_r is the conductivity (in S/m), Δ_e is the element volume (in m^3), k is the total number of elements in the different end components, J_e is the eddy current density (in A/m^2), and P_e is the eddy current loss (in W).

Fig. 4 shows the flux density on the inner surface of the magnetic screen at position F, position G, position K, position I, and position J under the different extension lengths of rotor end windings. In Fig. 4, the numbers 1, 2, 3, 4, and 5 represent 1st magnetic screen, 2nd magnetic screen, 3rd magnetic screen, 4th magnetic screen, and 5th magnetic screen.

The overall trend of the flux density on the inner surface of the magnetic screen increases gradually from position F to position J along the axial direction. At position F, the flux density on the inner surface of the magnetic screen is the lowest. When the extension length of rotor end windings is H=45 mm, H=85 mm, H=125 mm, H=165 mm, and H=205 mm, the flux densities of the magnetic screen at position F are 0.84T, 0.81T, 0.76T, 0.72T and 0.68T, respectively, 0.13T, 0.13T, 0.17T, 0.21T, and 0.22T lower than these

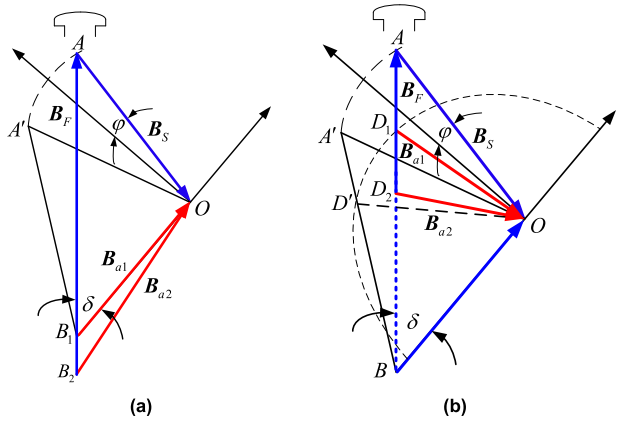

FIGURE 5. Vector diagrams. (a) Rotor end windings extension for the structure that is near the rotor. (b) Rotor end windings extension for the structure that is far away from the rotor.

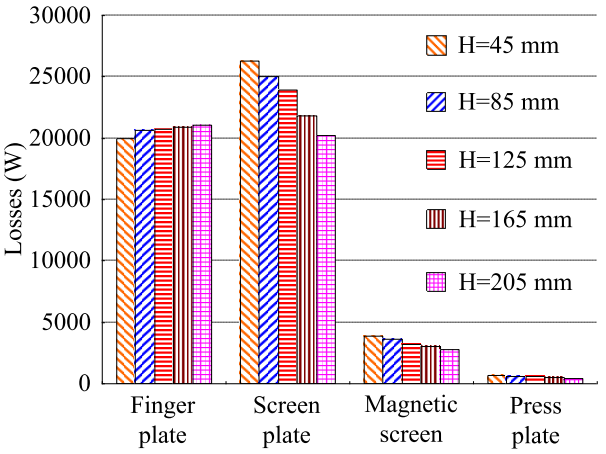

FIGURE 6. Loss values of the end components in the turbine generator end zone with magnetic screen under the different extension lengths of rotor end windings.

of the magnetic screen at position J. When the extension length of rotor end windings is H=205 mm, the flux density difference between position F and position J on the inner surface of the magnetic screen is the largest. As the extension length of rotor end windings increases, the flux density on the inner surface of the magnetic screen decreases gradually at the same position. When the extension length of rotor end windings increases from H=45 mm to H=205 mm, the change of flux density at position F is large and it is 0.16T. However, this change of flux density at position J is small and it is 0.07T. When the extension length of rotor end windings is H=45 mm, H=85 mm, H=125 mm, H=165 mm, and H=205 mm, the flux densities are 0.91T, 0.88T, 0.84T, 0.83T, and 0.8T at position K, respectively.

The flux densities of the end components that are generated from an armature reaction and field excitation are $\boldsymbol{B}_S$ and $\boldsymbol{B}_F$, respectively. The resultant of these two flux densities is denoted as $\boldsymbol{B}_a$. The subscripts 1 and 2 represent the normal structure and the increased extension of the rotor end windings, respectively. For the end region that is near the rotor, OB_1 represents the resultant flux density for the normal structure. OB_2 represents the resultant flux density with the increased extension of the rotor end windings. The resultant flux density is denoted as OB for the illustrations in Fig. 5(a). For the end region that is far away from the rotor, OD_1 is the resultant flux density for the normal structure. OD_2 is the resultant flux density with the increased extension of the rotor end windings. The resultant flux density is denoted as OD for the illustrations in Figs. 5(b).

As the finger plate is close to the rotor, the loss of the finger plate is mainly affected by the rotor. Therefore, the increased extension of the rotor end windings could cause an increase in the loss of the finger plate. However, as the other end components are far away from the rotor, their losses are mainly affected by the stator. Therefore, the increased extension of the rotor end windings could reduce the losses of the other end components. The losses of the screen plate, magnetic screen, and press plate decrease with the increased extension of the rotor end windings.

Fig. 6 shows the loss values of the end components in the turbine generator end zone with magnetic screen under the different extension lengths of rotor end windings.

As the extension length of rotor end windings increases, the loss values of press plate, screen plate, and magnetic screen decrease gradually. However, the loss value of finger plate increases gradually. When the extension length of rotor end windings is 45 mm, the loss values of the finger plate, screen plate, magnetic screen, and press plate are 19941W, 26278.4W, 3880.5W, and 654.7W, respectively. When the extension length of rotor end windings is 205 mm, the loss values of the finger plate, screen plate, magnetic screen, and press plate are 21064.9W, 20232.8W, 2799.6W, and 428.7W, respectively. The change of the loss value of the screen plate is obvious under the different extension lengths of rotor end windings in the turbine generator end zone with magnetic screen. The loss value of the screen plate when the extension length of rotor end windings is 45 mm is 1263W, 2360W, 4444.2W, and 6045.6W higher than that of the screen plate when the extension length of rotor end windings is 85 mm, 125 mm, 165 mm, and H=205 mm, respectively. Loss value of the screen plate when the extension length of rotor end windings is H=45 mm, H=85 mm, H=125 mm, H=165 mm, and H=205 mm is 25623.7W, 24398.1W, 23313.8W, 21359.5W, and 19804.1W higher than that of the press plate when the extension length of rotor end windings is H=45 mm, H=85 mm, H=125 mm, H=165 mm, and H=205 mm, respectively.

Fig. 7 shows the total loss of the end components under the different extension lengths of rotor end windings.

As the extension length of rotor end windings increases, the total loss of the end components decreases gradually. It indicates that the increase of the extension length of rotor end windings could reduce effectively the total loss of the end components. When the extension length of rotor end windings increases from H=45 mm to H=205 mm, the screen plate loss ratio decreases from 51.8% to 45.4%. However, the finger plate loss ratio increases from 39.3%

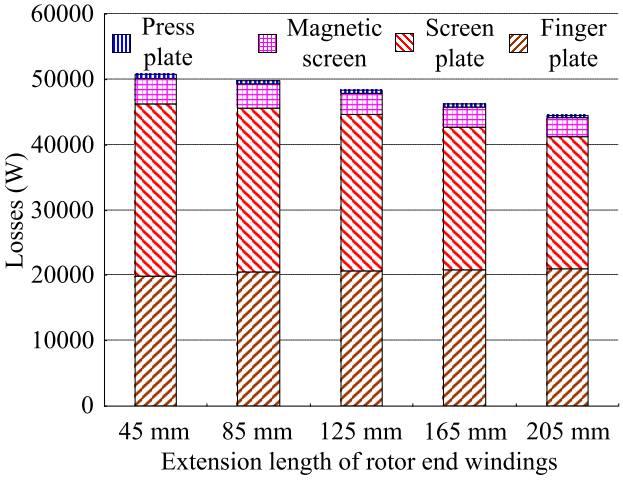

FIGURE 7. Total loss of the end components under the different extension lengths of rotor end windings.

to 47.3%. The magnetic screen loss ratio is about 6%-8%. The press plate loss ratio is lower than the other end components. The press plate loss ratio is almost constant, which is about 1%.

III. FLUID-THERMAL COUPLING MODEL IN THE LARGE TURBINE GENERATOR END ZONE WITH MAGNETIC SCREEN

To study the change of the complex fluid flow and the temperature of the end components in the turbine generator end zone with magnetic screen under the different extension lengths of rotor end windings, 3-D fluid-thermal coupling model of the 1250 MW turbine generator end zone with magnetic screen is established. Fig. 8 shows 3-D fluid-thermal coupling model of end zone. Fig. 8(a) gives the end components, water-pipe inlets, and fan outlet of the coupling model. Fig. 8(b) shows the other inlets and outlets of the coupling model. Fig. 9 gives the prototype of this turbine generator.

Fig. 10 gives the fluid velocities in all the inlets of end zone.

Fluid velocity of the ventilation duct inlet within stator end core is the largest and it is 52.19 m/s. However, fluid velocity of wind-board inlet is the smallest and it is 0.635 m/s. Fluid velocities of air-gap inlet, inlet of axial ventilation holes, and rectangle inlet are 45.27m/s, 45.9 m/s, and 13.34 m/s, respectively. These boundary conditions (provided by the manufacturer) are gained from the calculation of flow network. Pressure value of fan outlet is 950.6 Pa. The rated speed of turbine generator is 1500 r/min. The inlet velocity of water pipes is 0.822 m/s. The inlet temperature of water pipes is 51.2 °C and the other inlet temperatures are 54 °C.

IV. INFLUENCE OF THE EXTENSION LENGTH OF ROTOR END WINDINGS ON THERMAL FIELD IN THE TURBINE GENERATOR END ZONE WITH MAGNETIC SCREEN

In the 3-D fluid-thermal coupling model of the turbine generator end zone with magnetic screen, these values of fan outlet pressure and inlet velocity from flow network are used

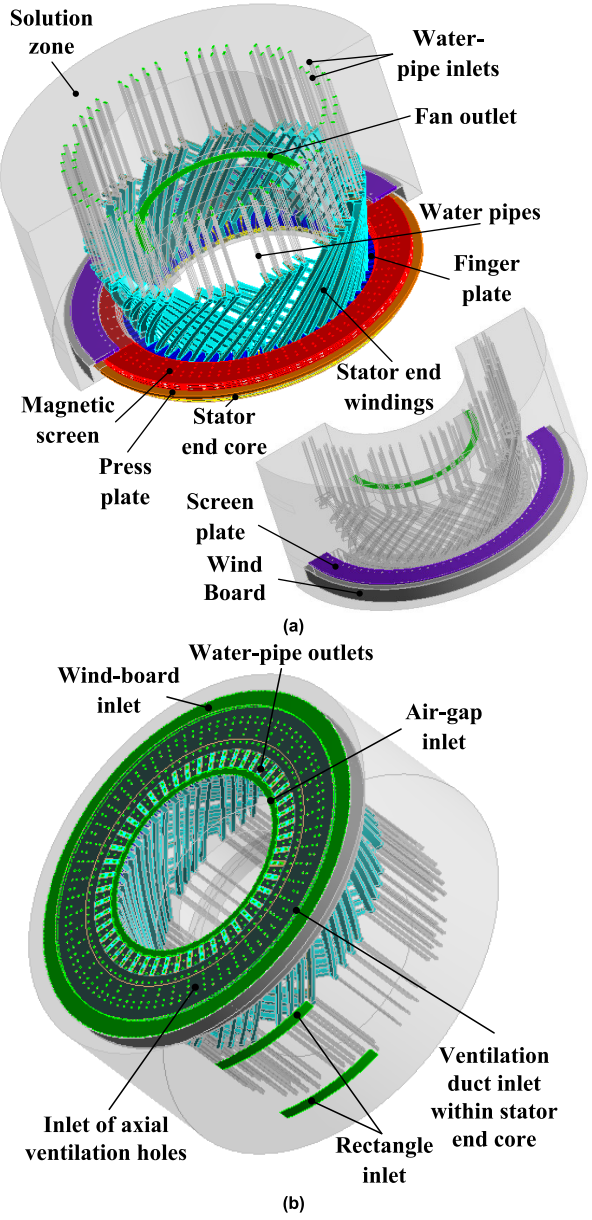

FIGURE 8. 3-D fluid-thermal coupling model of end zone. (a) End components, water-pipe inlets, and fan outlet of the coupling model. (b) The other inlets and outlets of the coupling model.

FIGURE 9. Prototype of this turbine generator.

as boundary conditions. Loss values of the end components from the 3-D transient electromagnetic field are used as heat

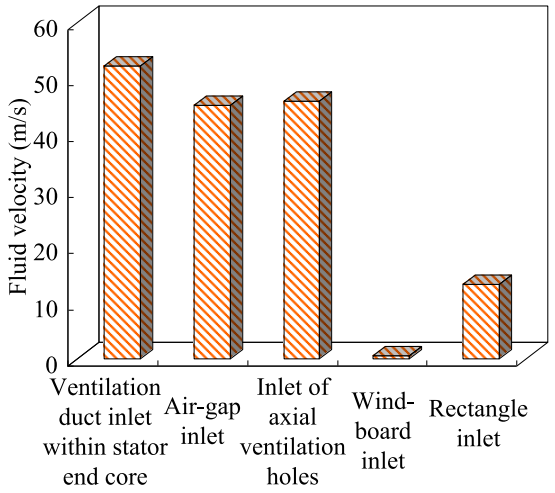

FIGURE 10. Fluid velocities in all the inlets of end zone.

source under the different extension lengths of rotor end windings. The simulation time of 3-D fluid-thermal coupling model is about 26 hours. The employed computer has 8 cores and 32 GB memories. Influence of the extension length of rotor end windings on the temperature of the end components in the large turbine generator end zone with magnetic screen is studied after solving the fluid-thermal coupling equations [17]–[24].

A. ANALYSIS OF FLUID VELOCITY AROUND THE FINGER PLATE IN THE TURBINE GENERATOR END ZONE WITH MAGNETIC SCREEN

Finger plate could fix the stator end core in the end zone of the turbine generator. Due to the influence of the complex electromagnetic field in the end zone, the loss value of the finger plate is high. The heat of the finger plate could be taken effectively away by the cooling fluid in the axial ventilation holes. Fig. 11 shows the fluid velocity distribution around the finger plate. In Fig. 11, the highest fluid velocity around the finger plate is 41.7 m/s, which appears in the axial ventilation holes of the finger-plate yoke. The high fluid velocity in the axial ventilation holes of the finger-plate yoke could take effectively away the heat of the finger-plate yoke. It results in a low temperature of the finger-plate yoke. The fluid velocity around the top of the finger-plate tooth is also high, which is about 21 m/s. It could decrease obviously the temperature of the finger-plate tooth. The fluid velocity around the top of the finger-plate tooth is higher than that around the bottom of the finger-plate tooth.

B. INFLUENCE OF THE EXTENSION LENGTH OF ROTOR END WINDINGS ON THERMAL FIELD IN THE LARGE TURBINE GENERAOTR END ZONE WITH MAGNETIC SCREEN

This paper focuses on the temperature distribution of the end components when the extension length of rotor end windings is 205 mm. The temperature change of the end components is compared and studied under the different extension lengths of

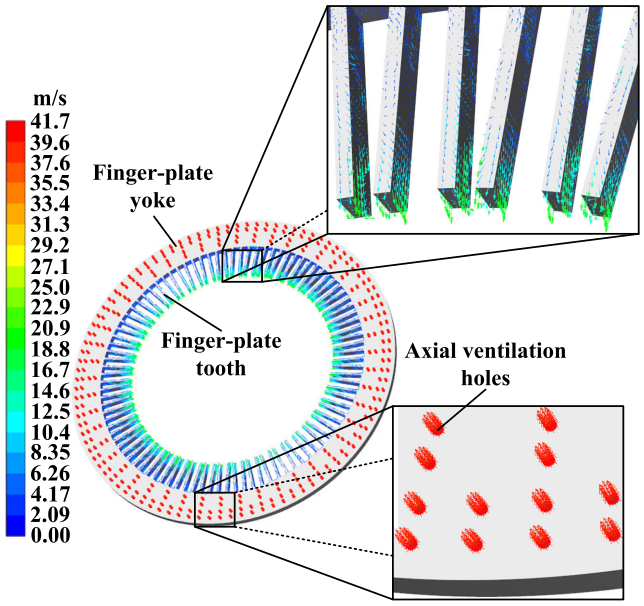

FIGURE 11. Fluid velocity distribution around the finger plate.

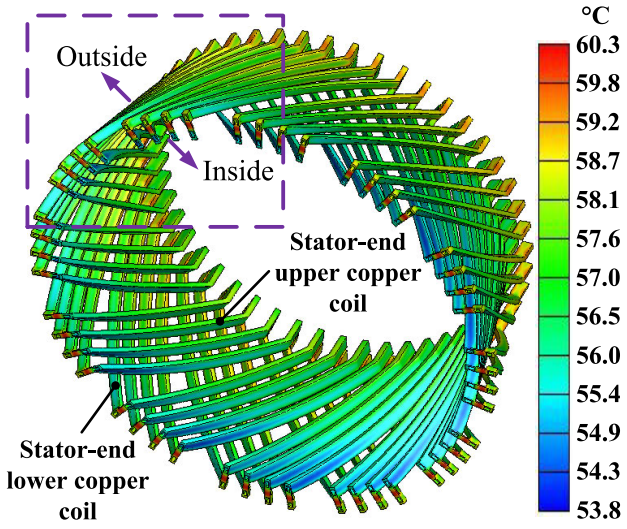

FIGURE 12. Temperature distribution of the stator-end copper coil when the extension length of rotor end windings is 205 mm.

rotor end windings. Fig. 12 gives the temperature distribution of the stator-end copper coil when the extension length of rotor end windings is 205 mm.

The highest temperature of the stator-end copper coil is 60.3°C when the extension length of rotor end windings is 205 mm, which appears in the nose of the stator-end copper coil. The cooling water inside the stator-end copper coil could take effectively away the heat of the stator-end upper copper coil in the end zone of the turbine generator. The temperature of the stator-end upper copper coil is lower than that of the stator-end lower copper coil. A high temperature appears in the junction of the stator-end copper coil and stator end core, and it is about 59.1 °C.

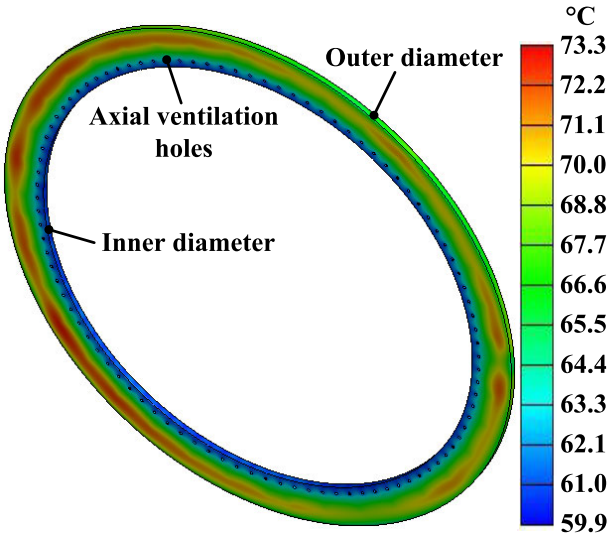

FIGURE 13. Temperature distribution of the screen plate when the extension length of rotor end windings is 205 mm.

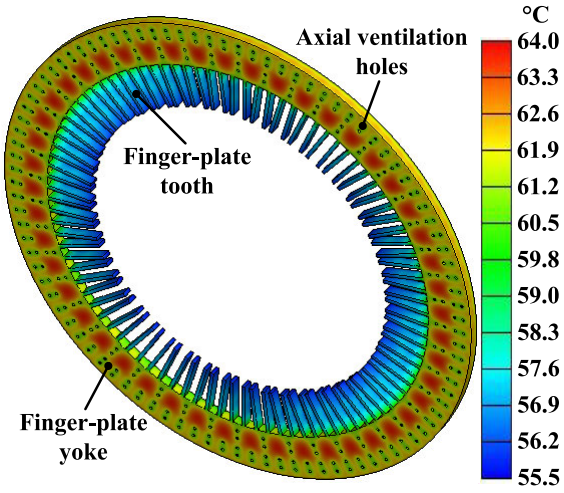

FIGURE 14. Temperature distribution of the finger plate when the extension length of rotor end windings is 205 mm.

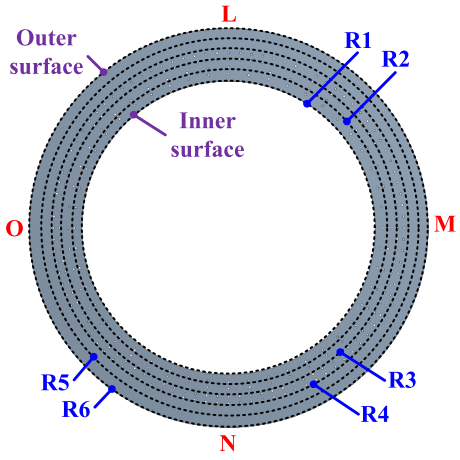

FIGURE 15. Location of these circumferential sample lines within the press plate.

Fig. 13 shows the temperature distribution of the screen plate when the extension length of rotor end windings is 205 mm.

The highest temperature of the screen plate is 73.3 °C when the extension length of rotor end windings is 205 mm, which appears around the outer diameter of the screen plate. The highest temperature of the screen plate when the extension length of rotor end windings is 205 mm is 5.7 °C, 4.5 °C, 3.5 °C, and 1.5 °C lower than that of the screen plate when the extension length of rotor end windings is 45 mm, 85 mm, 125 mm, and 165 mm, respectively. There are the axial ventilation holes in the inner diameter of the screen plate. The temperature in the inner diameter of the screen plate is relatively low and it is about 60.5 °C when the extension length of rotor end windings is 205 mm. The average temperature of screen plate when the extension length of rotor end windings is 205 mm is 4 °C, 3.2 °C, 2.4 °C, and 1.1 °C lower than that of the screen plate when the extension length of rotor end windings is 45 mm, 85 mm, 125 mm, and 165 mm, respectively. As the extension length of rotor end windings increases, the temperature drop of the screen plate is obvious. The highest temperature in the turbine generator end zone with magnetic screen always appears around the outer diameter of the screen plate under the different extension lengths of rotor end windings.

Fig. 14 shows the temperature distribution of the finger plate when the extension length of rotor end windings is 205 mm.

The highest temperature of the finger plate is 64 °C when the extension length of rotor end windings is 205 mm, which appears in the finger-plate yoke. Due to the cooling effect of the fluid from the axial ventilation holes of the stator core, the temperature of the finger-plate tooth is low. When the extension length of rotor end windings is 205 mm, the temperature of the finger-plate tooth is about 56.8 °C. The highest temperature of the finger plate when the extension length of rotor end windings is 205 mm is 0.35 °C, 0.12 °C, 0.1 °C, and 0.06 °C higher than that of the finger plate when the extension length of rotor end windings is 45 mm, 85 mm, 125 mm, and 165 mm, respectively. The average temperature of finger plate is 61.2 °C when the extension length of rotor end windings is 205 mm. The velocity of the cooling fluid in the axial ventilation holes of the finger-plate yoke is relatively high. It results in a lower temperature around the ventilation holes of the finger-plate yoke.

To study deeply the temperature distribution within the press plate, the press plate is divided evenly into five equal segments from the inner surface to the outer surface along the radial direction. Circumferential sample lines of radii R1=1.358 m, R2=1.455 m, R3=1.552 m, R4=1.649 m, R5=1.746 m, and R6=1.843 m are selected within the press plate along the radial direction. Fig. 15 shows the location of these circumferential sample lines within the press plate.

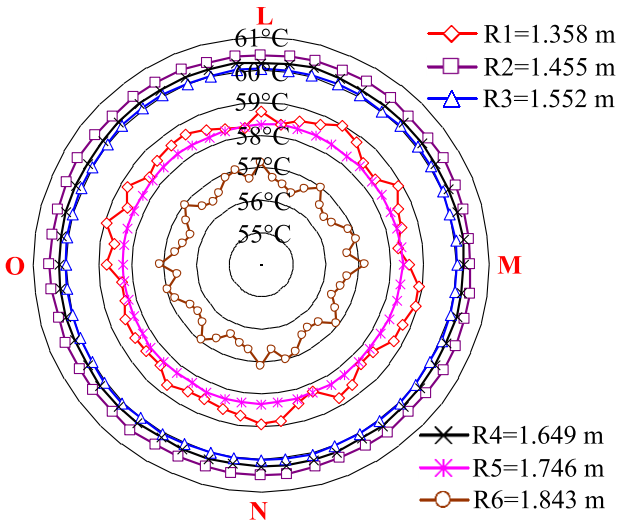

FIGURE 16. Temperature distribution of these sample lines within the press plate along the circumferential direction when the extension length of rotor end windings is 205 mm.

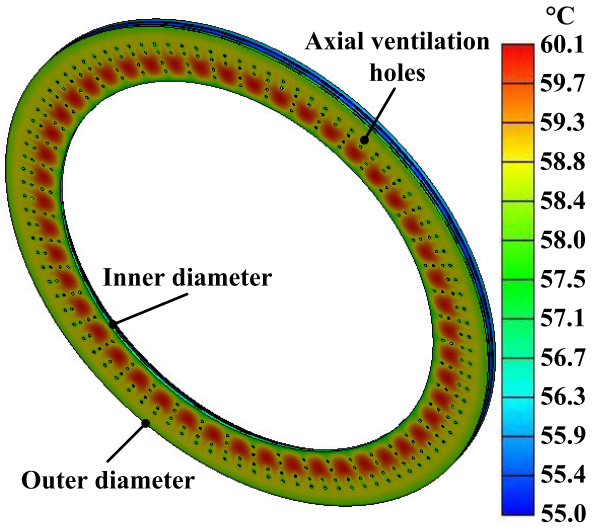

FIGURE 17. Temperature distribution of the magnetic screen when the extension length of rotor end windings is 205 mm.

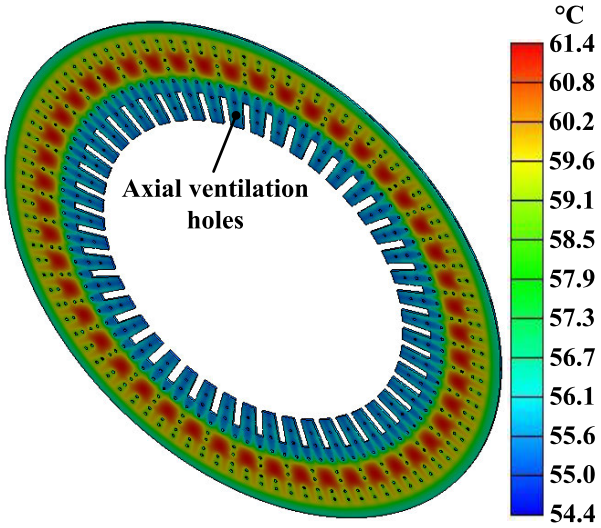

FIGURE 18. Temperature distribution of the 1st stator inner end core when the extension length of rotor end windings is 205 mm.

Fig. 16 shows the temperature distribution of these sample lines within the press plate along the circumferential direction when the extension length of rotor end windings is 205 mm.

When the extension length of rotor end windings is 205 mm, the temperature is basically the same in the radii R2, R3, and R4 within the press plate along the circumferential direction. The temperatures in the radii R2, R3, and R4 within the press plate are about 60.4 °C, 60 °C, and 60.2 °C, respectively. Due to the high fluid velocity around the outer diameter of the press plate, the lowest temperature appears in the radius R6=1.843 m and it is about 56.5 °C. Since the convective heat transfer occurs on the inner surface of the press plate, the temperature is relatively low in the radius R1=1.358 m within the press plate and it is about 58.7 °C. The temperature is about 58.3 °C in the radius R5=1.746 m within the press plate. The temperature difference is 3.9 °C between the radius R2=1.455 m and the radius R6=1.843 m within the press plate.

Fig. 17 shows the temperature distribution of the magnetic screen when the extension length of rotor end windings is 205 mm. In Fig. 17, the highest temperature of the magnetic screen appears around the inner diameter and it is 60.1 ° C when the extension length of rotor end windings is 205 mm. The highest temperatures of 1st magnetic screen, 2nd magnetic screen, 3rd magnetic screen, 4th magnetic screen, and 5th magnetic screen are 60.1 °C, 55.9 °C, 55.8 °C, 55.9 °C, and 56.5 °C when the extension length of rotor end windings is 205 mm, respectively, 0.01 °C, 0.4 °C, 0.4 °C, 0.5 °C, and 0.6 °C lower than these of 1st magnetic screen, 2nd magnetic screen, 3rd magnetic screen, 4th magnetic screen, and 5th magnetic screen when the extension length of rotor end windings is 45 mm. The extension length of rotor end windings has little effect on the temperature of the magnetic screen. The average temperatures of 1st magnetic screen, 2nd magnetic screen, 3rd magnetic screen, 4th magnetic screen, and 5th magnetic screen are 57.9 °C, 55.6 °C, 55.4 °C, 55.5 °C, and 56.1 °C when the extension length of rotor end windings is 205 mm.

Fig. 18 gives the temperature distribution of the 1st stator inner end core when the extension length of rotor end windings is 205 mm.

It can be seen from Fig. 18 that the highest temperature of the 1st stator inner end core is 61.4 °C when the extension length of rotor end windings is 205 mm. The cooling fluid in the axial ventilation holes could take effectively away the heat of the 1st stator inner end core tooth. The temperature of the 1st stator inner end core tooth is relatively low and it is about 56 °C. Due to the influence of the temperature of the end components, the temperature of the 1st stator inner end core yoke is higher than that of the 1st stator inner end core tooth.

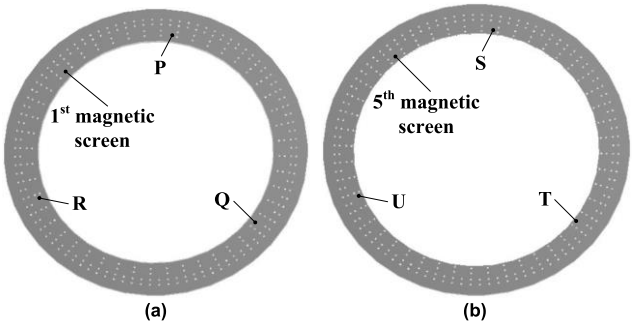

FIGURE 19. Positions of three temperature sensors in the 1st magnetic screen and 5th magnetic screen. (a) 1st magnetic screen. (b) 5th magnetic screen.

TABLE 1. Measured values and calculated results in the 1 st magnetic screen and 5 th magnetic screen under the no-load operation when the extension length of rotor end windings is 125 mm.

Magnetic screen	1st magnetic screen			5th magnetic screen		
Measured points	Point P	Point Q	Point R	Point S	Point T	Point U
Measured values (°C)	47.4	47.9	46.2	47.9	46.2	49.5
Calculated results (°C)	46.77	46.77	46.78	46.56	46.55	46.56

The temperature is about 58 °C in the outer diameter of the 1st stator inner end core. The difference between the highest temperature and the lowest temperature of the 1st stator inner end core is 7 °C.

C. CALCULATED RESULTS AND MEASURED VALUES

To verify the accuracy of the calculated results, three temperature sensors are embedded at 120° angles along the circumference in the 1st magnetic screen and 5th magnetic screen, respectively. Fig. 19 shows the positions of three temperature sensors in the 1st magnetic screen and 5th magnetic screen. Table 1 gives the measured values and calculated results in the 1st magnetic screen and 5th magnetic screen under the no-load operation when the extension length of rotor end windings is 125 mm. The measured values are close to calculated results. It proves that the calculation method and calculated results are reliable and accurate.

V. CONCLUSION

In this paper, influence of the extension length of rotor end windings on the electromagnetic and thermal fields in the large turbine generator end zone with magnetic screen is investigated. The main conclusions are as follows.

1) As the extension length of rotor end windings increases, the loss value of finger plate increases gradually. However, the loss values of press plate, screen plate, and magnetic screen decrease gradually. The total loss of the end components also decreases gradually. When the extension length of rotor end windings increases from H=45 mm to H=205 mm, the screen plate loss ratio decreases from 51.8% to 45.4%. However, the finger plate loss ratio increases from 39.3% to 47.3%. The magnetic screen loss ratio and the press plate loss ratio change a little.

2) The highest fluid velocity around the finger plate is 41.7 m/s, which appears in the axial ventilation holes of the finger-plate yoke. The fluid velocity around the top of the finger-plate tooth is also high, which is about 21 m/s. The fluid velocity around the top of the finger-plate tooth is higher than that around the bottom of the finger-plate tooth. Fluid velocity distribution around each finger-plate tooth is basically the same along the circumferential direction.

3) The highest temperature in the turbine generator end zone with magnetic screen always appears around the outer diameter of the screen plate under the different extension lengths of rotor end windings. As the extension length of rotor end windings increases, the temperature drop of the screen plate is obvious. However, the temperature changes of the finger plate, press plate, and magnetic screen are small. The highest temperature of the screen plate when the extension length of rotor end windings is 205 mm is 5.7 °C lower than that of the screen plate when the extension length of rotor end windings is 45 mm.

REFERENCES

[1] R. Albanese, F. Calvano, G. D. Mut, F. Ferraioli, A. Formisano, F. Marignetti, R. Martone, A. Romano, G. Rubinacci, A. Tamburrino, and S. Ventre, "Coupled three dimensional numerical calculation of forces and stresses on the end windings of large turbo generators via integral formulation," *IEEE Trans. Magn.*, vol. 48, no. 2, pp. 875–878, Feb. 2012.

[2] M. Fujita, T. Ueda, T. Tokumasu, K. Nagakura, M. Kakiuchi, and T. Otaka, "Eddy current analysis in the stator end structures of large capacity turbine generators," in *Proc. Int. Conf. Electr. Mach. Syst.*, Nov. 2009, pp. 1–6.

[3] G. Xu, Y. Zhan, X. Liu, H. Zhao, and Y. Luo, "Influence of rotor damping structure on speed fluctuation and asynchronous operating ability of turbogenerators with loss of excitation," *IEEE Trans. Ind. Electron.*, vol. 66, no. 2, pp. 1012–1022, Feb. 2019.

[4] M. Fratila, A. Benabou, A. Tounzi, and M. Dessoude, "Iron loss calculation in a synchronous generator using finite element analysis," *IEEE Trans. Energy Convers.*, vol. 32, no. 2, pp. 640–648, Jun. 2017.

[5] M. Šašić, B. Lloyd, and A. Elez, "Finite element analysis of turbine generator rotor winding shorted turns," *IEEE Trans. Energy Convers.*, vol. 27, no. 4, pp. 930–937, Dec. 2012.

[6] S. Li, C. Gong, N. A. Gallandat, J. R. Mayor, and R. G. Harley, "Implementation of surface impedance boundary conditions in the quasi three-dimensional finite-difference simulations of generator end regions," in *Proc. IEEE Int. Electr. Mach. Drives Conf. (IEMDC)*, May 2017, pp. 1–7.

[7] S. Li, C. Gong, N. A. Gallandat, J. R. Mayor, and R. G. Harley, "Analyzing the impact of press plate structure on the flux and loss distributions in the end region of large generators by transient 3-dimensional finite-element method with an improved core loss model," in *Proc. IEEE Int. Electr. Mach. Drives Conf. (IEMDC)*, May 2017, pp. 1–8.

[8] S. Li, C. Gong, J. R. Mayor, R. G. Harley, and T. G. Habetler, "Efficient calculation of the strand eddy current loss distributions in the end stepped-stator region of large synchronous generators," in *Proc. IEEE Energy Convers. Congr. Expo. (ECCE)*, Sep. 2018, pp. 1783–1789.

[9] S. Li, C. Gong, L. Du, J. R. Mayor, R. G. Harley, and T. G. Habetler, "Parametric study for the design of the end region of large synchronous generators based on three-dimensional transient finite element analysis," in *Proc. IEEE Energy Convers. Congr. Expo. (ECCE)*, Sep. 2018, pp. 7356–7362.

[10] S. Li, C. Gong, L. Du, J. R. Mayor, R. G. Harley, and T. G. Habetler, "Fast calculation of the magnetic field and loss distributions in the stator core end packets and finger plates of large synchronous generators," in *Proc. IEEE Energy Convers. Congr. Expo. (ECCE)*, Sep. 2018, pp. 822–828.

[11] S. Wróblewski and A. Napieralski, "A multichannel measurement system for online turbogenerator vibration diagnostics," *IEEE Trans. Energy Convers.*, vol. 27, no. 4, pp. 978–983, Dec. 2012.

[12] J. Han, B. Ge, and W. Li, "Influence of magnetic permeability of the press plate on the loss and temperature of the end part in the end region of a turbogenerator," *IEEE Trans. Ind. Electron.*, vol. 66, no. 1, pp. 162–171, Jan. 2019.
[13] S. K. Harmukh, K. S. Haran, S. Salon, and J. Stein, "Root cause analysis of arcing in retaining rings of turbogenerators," *IEEE Trans. Ind. Appl.*, vol. 53, no. 3, pp. 3129–3136, May 2017.
[14] W. Yucai, M. Minghan, and L. Yonggang, "A new detection coil capable of performing online diagnosis of excitation winding short-circuits in steam-turbine generators," *IEEE Trans. Energy Convers.*, vol. 33, no. 1, pp. 106–115, Mar. 2018.
[15] O. Biro, K. Preis, and K. R. Richter, "Various FEM formulations for the calculation of transient 3D eddy currents in nonlinear media," *IEEE Trans. Magn.*, vol. 31, no. 3, pp. 1307–1312, May 1995.
[16] D. Lin, P. Zhou, W. N. Fu, Z. Badics, and Z. J. Cendes, "A dynamic core loss model for soft ferromagnetic and power ferrite materials in transient finite element analysis," *IEEE Trans. Magn.*, vol. 40, no. 2, pp. 1318–1321, Mar. 2004.
[17] S. Utegenova, F. Dubas, M. Jamot, R. Glises, B. Truffart, D. Mariotto, P. Lagonotte, and P. Desevaux, "An investigation into the coupling of magnetic and thermal analysis for a wound-rotor synchronous machine," *IEEE Trans. Ind. Electron.*, vol. 65, no. 4, pp. 3406–3416, Apr. 2018.
[18] R. Camilleri, P. Beard, D. A. Howey, and M. D. McCulloch, "Prediction and measurement of the heat transfer coefficient in a direct oil-cooled electrical machine with segmented stator," *IEEE Trans. Ind. Electron.*, vol. 65, no. 1, pp. 94–102, Jan. 2018.
[19] S. Nategh, H. Zhang, O. Wallmark, A. Boglietti, T. Nassen, and M. Bazant, "Transient thermal modeling and analysis of railway traction motors," *IEEE Trans. Ind. Electron.*, vol. 66, no. 1, pp. 79–89, Jan. 2019.
[20] P. Taras, G.-J. Li, Z.-Q. Zhu, M. P. Foster, and D. A. Stone, "Combined multiphysics model of switched flux PM machines under fault operations," *IEEE Trans. Ind. Electron.*, vol. 66, no. 9, pp. 6737–6745, Sep. 2019.
[21] H. Vansompel, A. Yarantseva, P. Sergeant, and G. Crevecoeur, "An inverse thermal modeling approach for thermal parameter and loss identification in an axial flux permanent magnet machine," *IEEE Trans. Ind. Electron.*, vol. 66, no. 3, pp. 1727–1735, Mar. 2019.
[22] J. G. Amoros, P. Andrada, B. Blanque, and M. Marin-Genesca, "Influence of design parameters in the optimization of linear switched reluctance motor under thermal constraints," *IEEE Trans. Ind. Electron.*, vol. 65, no. 2, pp. 1875–1883, Feb. 2018.
[23] S. Ulbrich, J. Kopte, and J. Proske, "Cooling fin optimization on a TEFC electrical machine housing using a 2-D conjugate heat transfer model," *IEEE Trans. Ind. Electron.*, vol. 65, no. 2, pp. 1711–1718, Feb. 2018.
[24] X. Guo, Q. Wang, R. Shang, F. Chen, W. Fu, and W. Hua, "Design and analysis of a novel synthetic slot dual-PM machine," *IEEE Access*, vol. 7, pp. 29916–29923, 2019.

HAN JICHAO was born in Harbin, China, in 1986. He received the B.S., M.S., and Ph.D. degrees in electrical machinery and appliance from the Harbin University of Science and Technology, Harbin, China, in 2010, 2013, and 2015, respectively. He is currently an Associate Professor with the Harbin University of Science and Technology. He is the author or coauthor of more than 20 refereed technical articles in IEEE TRANSACTIONS and IET proceedings. He holds more than 20 invention patents. His research interests include research on ventilation cooling, electromagnetics, fluids, and thermal analysis on large electrical generators, particularly in large turbogenerators.

WANG CHAO was born in Yichun, China, in 1997. He received the B.S. degree in electrical engineering and automation from Suihua University, Suihua, China, in 2019. He is currently pursuing the M.S. degree in electrical machinery and appliance with the Harbin University of Science and Technology, Harbin, China. He researches on the electromagnetics and thermal analysis on electrical generator.

WANG YANG was born in Shanxi, China, in 1997. He received the B.S. degree in electrical engineering and automation from the Taiyuan University of Science and Technology, Shanxi, in 2019. He is currently pursuing the M.S. degree in electrical machinery and appliance with the Harbin University of Science and Technology, Harbin, China. He researches on the ventilation cooling, fluids, and thermal analysis on electrical generator.

SUN YUTIAN was born in 1963. He received the B.S. and M.S. degrees in electrical machinery and appliance from the Harbin University of Science and Technology, Harbin, China, in 1984 and 1987, respectively, and the Ph.D. degree in electrical machine from the Shenyang University of Technology, Shenyang, in 1998. He is currently the Deputy Chief Designer of Harbin Electric Machinery Company Ltd. He is also engaged in the design of large generator.

ZHENG PING received the B.S., M.S., and Ph.D. degrees in electrical engineering from the Harbin Institute of Technology, Harbin, China, in 1992, 1995, and 1999, respectively. Since 1995, she has been with the Harbin Institute of Technology, where she has been a Professor, since 2005. She has authored or coauthored more than 220 published refereed technical articles and four books. She is the holder of 56 Chinese invention patents. Her current research interests include electric machines and control, hybrid electric vehicles, and unconventional electromagnetic devices.